

Additively Manufactured Microfluidics-Based “Peel-and-Replace” RF Sensors for Wearable Applications

Wenjing Su, *Student Member, IEEE*, Benjamin S. Cook, *Graduate Student Member, IEEE*, and Manos M. Tentzeris, *Fellow, IEEE*

Abstract—This paper demonstrates the first-of-its-kind additively manufactured microfluidics-based flexible RF sensor, combining microfluidics, inkjet-printing technology, and soft lithography, which could potentially enable the first “real-world” wearable “smart skin” applications. A low-cost, rapid, low-temperature, and zero-waste fabrication process is introduced, which can be used to realize complex microfluidic channel networks with virtually any type of sensing element embedded. For proof-of-concept purposes, a reusable and flexible microfluidics sensor was prototyped using this process, which only requires 0.6- μL fluid volume to produce a 44% frequency shift between an empty ($\epsilon_r = 1$) and a water-filled channel ($\epsilon_r = 73$), demonstrating a sensitivity that is higher than most previously reported microfluidics-based microwave sensors. Seven different fluids were used to measure the sensitivity of the prototype and an overall sensitivity of 24%/log(ϵ_r) was observed. The “peel-and-replace” capability of the presented sensor not only facilitates the cleaning process for sensor reusability, but it also enables sensitivity tunability. For bent/conformed configurations, the sensor’s functionality is good even for a bending radius down to 7 mm, demonstrating its great flexibility. After bending multiple times, the sensor still exhibits a very good performance repeatability, which verifies its reusability feature. The introduced additively manufactured RF microfluidics-based sensor would be well suited for numerous wearable and conformal fluid sensing applications (e.g., bodily fluids analyzing and food monitoring), while it could also be utilized in a variety of microfluidics-reconfigurable microwave components.

Index Terms—Additive manufacturing, emerging applications for RF/microwaves, fabrication technology, microfluidics, RF sensors, wearable sensors.

I. INTRODUCTION

WEARABLE sensors and “smart skins” have drawn a lot of attention from the research community and the industry recently [1]. As healthcare costs have dramatically increased over the last 10–15 years and the global population

is growing and aging, we have reached a point where remote biomonitors is overtaking the traditional hospital-focused model and has become the predominant way of real-time patient-progress tracking [2]. For instance, the real-time monitoring of bodily fluids, such as tears, sweat, urine, and blood, performed by the patient himself or by a medical center, could be an excellent way to track patient health status and alert the patient in time to prevent any life-threatening situations. On the one hand, bodily fluid real-time monitoring cannot be easily realized in the current hospital-focused model due to the difficulties associated with sample generation, collection, and delivery [3]. On the other hand, this task can be easily undertaken by using wearable fluid sensors featuring characteristics such as miniaturization, low-cost production, and flexibility. In this background, micro-total-analysis (μTAS) or lab-on-a-chip (LOC) [4] as well as microfluidics are naturally being important technical tools to realize desired wearable sensors [5].

Due to its capability of manipulating extremely small quantities of liquids and due to its compact size that enables easily embedding into various devices, microfluidics technology has been widely used in biomedical sensing, manufacturing control, chemical assay, and other lab-on-chip applications in the past decades [6]. The first microfluidic prototype, developed in the early 1990s, was fabricated in silicon and glass by photolithography, a conventional planar manufacturing technique, that is generally expensive and environmentally unfriendly. Recently, [7]–[9] reported the successful lower cost fabrication of flexible microfluidics using the soft-lithography technique. The authors used poly (dimethylsiloxane) (PDMS), an elastomer with great compatibility with many organic solvents, that are commonly used in numerous applications [10]. However, this mold-based method is still strongly relying on photolithography to fabricate the mold, which raises the manufacturing cost. Recent years have witnessed an increasing number of novel and low-cost fabrication approaches being proposed to address these issues.

Inkjet printing, a low-cost rapid additive manufacturing technique, has been recently introduced in the microfluidics fabrication process [11], [12]. Most prior research efforts of inkjet-printed microwave sensors/tunable elements [12]–[16] took advantage of the inkjet-printing technique only for sealing the microfluidic channels and patterning the conductive structures, but they still required other subtractive manufacturing

Manuscript received October 17, 2015; revised April 18, 2016; accepted April 22, 2016. Date of publication May 13, 2016; date of current version June 2, 2016. This work was supported by the National Science Foundation (NSF) and by the Defense Threat Reduction Agency (DTRA).

W. Su and M. M. Tentzeris are with the School of Electrical and Computer Engineering, Georgia Institute of Technology, Atlanta, GA 30332 USA (e-mail: wenjing.su.gatech@gmail.com; etentze@ece.gatech.edu).

B. S. Cook was with the School of Electrical and Computer Engineering, Georgia Institute of Technology, Atlanta, GA, 30332 USA. He is now with Kilby Labs, Texas Instruments Incorporated, Dallas, TX 75243 USA (e-mail: benjamin.cook@ti.com).

Color versions of one or more of the figures in this paper are available online at <http://ieeexplore.ieee.org>.

Digital Object Identifier 10.1109/TMTT.2016.2560177

techniques such as laser etching to fabricate the channels. This paper presents a new approach, which eliminates any subtractive manufacturing step for the first time and enables the fabrication of complex microfluidics networks with any type of sensing element embedded in virtually any substrate at low cost. By replacing all the subtractive photolithography steps in the soft-lithography process with the inkjet-printing technique, a new microfluidics fabrication process, which features a much lower cost and a sufficient resolution, is presented in this paper, bringing the traditional soft lithography process out of the cleanroom and making microfluidics more accessible for daily applications. This new process also features numerous advantages over formerly published inkjet-printed microfluidic microwave sensors [13]–[16] as it has no waste; it is capable of realizing flexible microfluidics; it can fabricate ultra-small channels so that capillary action can feed fluids to the channel; it enables “peel-and-replace,” which means the sensor prototypes can switch sensitivity if needed. This paper also presents a proof-of-concept reusable, “peel-and-replace” and flexible microfluidics RF sensor prototype, which clearly demonstrates the advantages of the proposed technology in various wearable applications.

This paper is organized as follows. Section II discusses the microfluidics sensor fabrication process based on additive manufacturing. Sections III and IV discuss the theoretical principle of operation and the experimental verification of the performance of a proof-of-concept prototype fabricated using the proposed process.

II. FABRICATION

The fabrication process introduced in this paper demonstrates a novel technological platform that can be used to fabricate complex microfluidic channel networks with any type of sensing element embedded. This method can also be used to mount “on demand” microfluidics on silicon, taking full advantage of the microfluidics capabilities in packaging and liquid-reconfigurable electronics. The proposed process also features low-temperature, rapid-prototyping, highly controlled, eco-friendly, and zero-waste properties.

A typical microfluidics-based sensor, such as the prototype shown in Fig. 1, consists of two parts: the microfluidics part for the manipulation of the test fluids and the electrical part for sensing. The sensor fabrication process, as shown in Fig. 2, includes five steps. Steps 1 and 2 construct the microfluidics part; steps 3 and 4 print the electrical part; step 5 integrates the two parts together and completes the prototype.

The materials used for the proof-of-concept prototype were the Sylgard 182 Silicone Elastomer Kit (Dow Corning Corporation, Midland, MI, USA), the raw material of PDMS, for the construction of the microfluidic channel; a sheet of 0.127-mm-thick polyethylene terephthalate (PET) (DuPont Teijin Films, Chester, VA, USA) onto which the metallized layer is printed; ANP Silver-Jet 55LT-25C silver nanoparticle ink (Advanced Nano Products, Sejong, South Korea) for the inkjet printing of the conductive features; an SU-8 polymer solution (MicroChem, Newton, MA, USA) for the printing of the mold of the microfluidics, as well as for

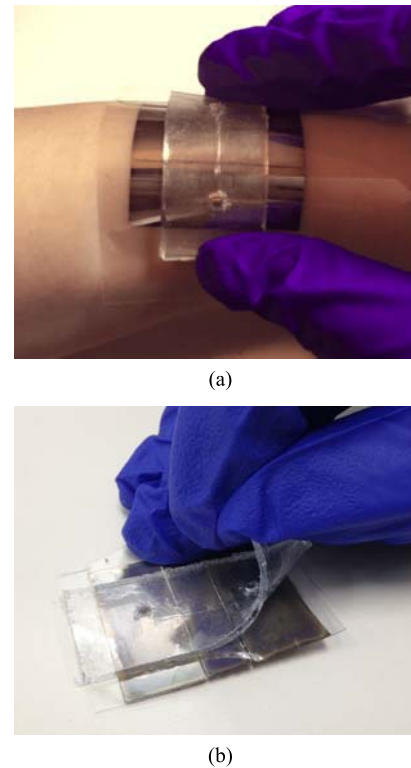


Fig. 1. (a) Photograph demonstrating the attachment of the microfluidic sensor prototype on the wrist. (b) Photograph of the fabricated prototype with the PDMS sheet (microfluidic part) partially peeled off from the PET sheet (electrical part) to illustrate the “peel-and-replace” capability.

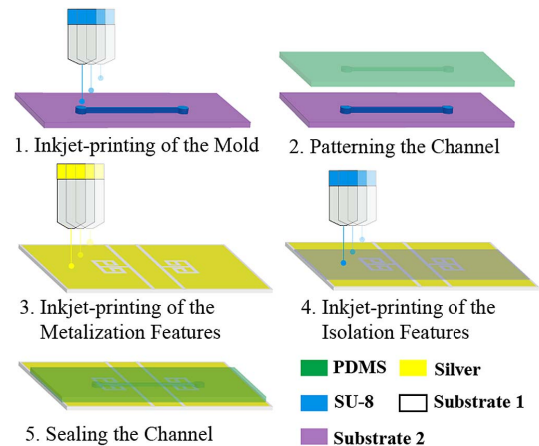


Fig. 2. Step-by-step fabrication process.

the function of isolating the conductive pattern from a direct contact with the fluid; a sheet of glass (Corning, Corning, NY, USA) for the mold fabrication; and Circuit Works 60 Minute Cure Conductive Epoxy (Chemtronix, Kennesaw, GA, USA) for the attachment of RF connectors.

A. Inkjet Printing of the Mold

The first step covers the inkjet printing of the microfluidic channel, which defines the shape of the fluids’ moving path. In traditional soft lithography processes for the microfluidics fabrication, the fabrication of the mold is carried out by

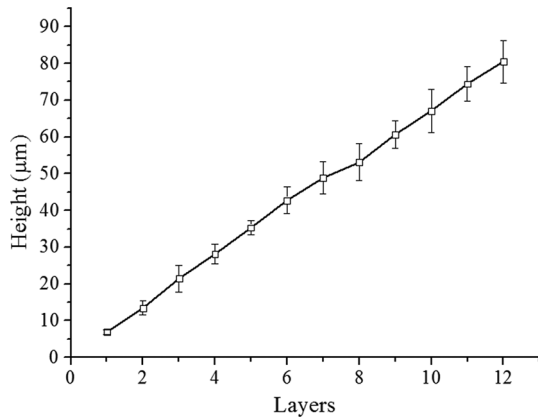


Fig. 3. SU-8 height calibration characteristics and repeatability. The line in the graph shows the average height values for ten samples/number of layers and the error bar shows the standard deviation of the heights.

photolithography in the cleanroom environment, which is the most environmental unfriendly and the most costly step in the whole process. In this paper, inkjet printing, an additive manufacturing technique, was utilized to fabricate a state-of-the-art mold, which reduces drastically the cost of fabricating microfluidic channels. Inkjet-printed SU8 has been already utilized in recent research for multilayer structures [17], [18], and was used in this paper to pattern the mold. SU-8 is a negative epoxy-type near-UV photoresist that can be as thick as 2 mm with an aspect ratio > 20 in UV-lithography [19], and thus constitutes an excellent candidate for constructing the mold of the microfluidic channel.

Before printing, the glass was cleaned by an acetone solution, an ethanol solution, and a cool dry air flow in sequence. Although in the presented prototype the mold was printed on glass, any material with a smooth surface could be utilized as substrate 2 in Fig. 2. To achieve a surface energy, which accommodates better the ink drops, a 2-min UV-ozone treatment was applied to the cleaned glass with a UVO cleaner (Jelight Company Inc., Irvine, CA, USA). The channel was inkjet-printed with a 10-pL cartridge, a drop spacing of $20 \mu\text{m}$, a print head temperature of 40°C , a jetting frequency of 5 kHz, and a platform at room temperature (around 25°C). Numerous layers of inkjet-printed SU8 with a thickness of around a $6\text{--}7\text{-}\mu\text{m}$ /printed layer [17] were used to accurately define the vertical dimension of the printed mold of the microfluidic channel. To further investigate the vertical fabrication accuracy of the printed SU-8, 1–12 layers of $7 \times 0.5 \text{ mm}^2$ rectangular patches were printed for ten different samples and the measured results are shown in Fig. 3. A good linearity with a relatively small standard deviation can be observed, which verifies a high enough resolution in the vertical direction with a very good repeatability. For the proof-of-concept prototype presented in this paper, ten layers of SU-8 were printed to achieve a total channel height of $68 \mu\text{m}$. As inkjet-printing deposits liquid phase material, the printed pattern obtains a semi-elliptical cross section, which facilitates the detachment of the mold and the PDMS sheet.

In addition to the channel, a $20\text{-}\mu\text{m}$ -thick 1.5-mm-diameter circular SU-8 pad was printed and a 1.5-mm-thick place holder

was placed on the SU-8 pad to reserve the openings for the fluids to enter and leave the channel. SU-8 functioned as the epoxy and glued the place holder on the glass.

B. Patterning the Channel

PDMS can be shaped as the negative pattern of the mold based on the traditional soft lithography technology [7]. The Sylgard 182 Silicone Elastomer Kit contains two parts: the base and the curing agent, which were mixed with a mixing ratio of 10:1 by weight. The mixture was poured to a container until overflow and was degassed with vacuum for three rounds. The container was a small box without a lid and had a height equal to that of the placeholder, which would eventually become the thickness of the PDMS sheet. The glass substrate was then flipped and squeezed to cover the container as a lid with the SU-8 pattern on the bottom side. To cure PDMS, the container and the lid were clipped together and heated at 100°C in a Thermo Scientific oven for 75 min. After being cooled down, the PDMS sheet was detached from the mold.

C. Inkjet Printing of the Metallization and Isolation Features

The metallization features were inkjet printed on a PET sheet utilizing ANP silver ink with a 10-pL cartridge, a drop spacing of $20 \mu\text{m}$, a print head temperature of 38°C , a jetting frequency of 5 kHz, and a platform temperature of 50°C to accelerate ink drying between each layer. PET in the presented prototype (substrate 1 in Fig. 2) can be substituted by any substrate with inkjet-printing capability including paper, silicon, liquid crystal polymer (LCP), and glass. A total of four layers of silver ink were printed in order to obtain the optimal sheet resistance of 0.03 Ohm/square . After printing, the PET sheet with the printed silver pattern was dried at room temperature. Fast drying in a higher temperature may lead to an uneven distribution of the silver nanoparticles, which could result in a nonuniformity of the conductivity values along the trace and thus should be avoided. After the ink dried, the PET sheet was sintered at 180°C in the oven for 1 h.

SU-8 has a very high chemical resistance and thus it has been frequently involved in microchannel fabrications [20], which makes it an ideal material for the isolation layer. To isolate the fluid under test from the silver pattern, a layer of $6\text{-}\mu\text{m}$ -thick SU-8 polymer was inkjet printed on top of the silver using the same setting as in the printing of the mold.

D. Sealing the Channel

PDMS can be sealed against a smooth surface taking advantage of Van Der Waals forces, which are caused by the microscopic attraction between two closely spaced macroscopic surfaces [6]. On the one hand, this reversible sealing features a strong enough bonding to prevent fluid leakage and to handle the pressure in the capillary action. On the other hand, reversible sealing gives the prototype a unique “peel-and-replace” capability. The microfluidic part can be easily peeled off from the electrical part if needed, as shown in Fig. 1(b), thus making sensitivity switching possible, as microfluidic parts with different channel designs can be easily attached

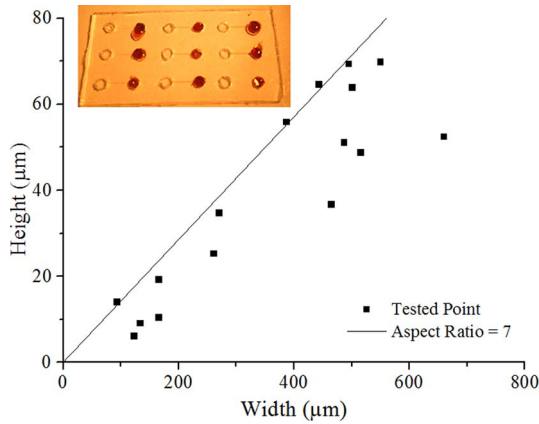


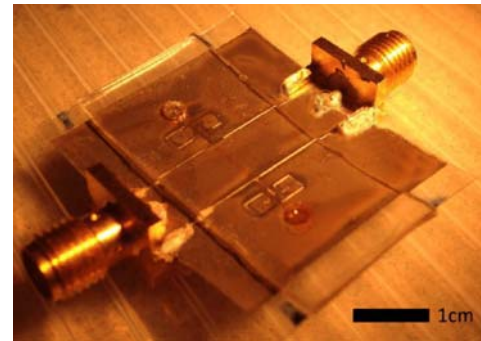
Fig. 4. Tests of the realized dimensions with the proposed fabrication process. The dots represent successful individual tests. The line in the graph shows the lower limit of the successful fabricated aspect ratio. The small inserted photograph in the figure gives the reader a glance of the testing matrix.

to the same RF pattern/structure (electrical parts). Various combinations of microfluidic and electrical parts can enable a large degree of reconfigurability and functionality of the RF system. Moreover, reversible sealing also simplifies the cleaning process between two consecutive uses, and thus enables reusability. The prototype can be demounted and cleaned part-by-part to remove any leftovers from the latest test.

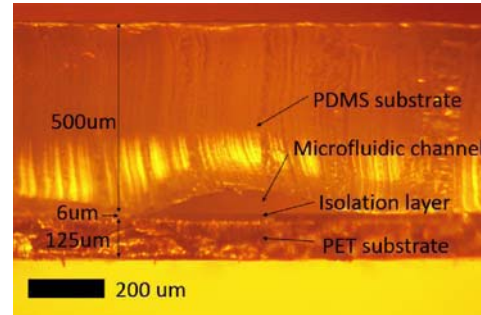
To produce a sufficient Van Der Waals force, the PDMS and PET were squeezed together until no air bubble was left. Before sealing, two preparatory steps were performed to enhance a successful bonding: firstly, the PDMS and PET sheet were cleaned by ethanol and dried by air flow; secondly, the two sheets were treated with UV-ozone for 5 min to achieve enhanced bonding and hydrophilicity properties. Four markers are placed in both microfluidic and electrical parts to facilitate their better alignment. At least 30 times of peel and replace capability are expected with appropriate cleaning.

To explore the limits of the proposed channel fabrication process, various channel sizes were fabricated and tested, as indicated in Fig. 4. The minimum aspect ratio (width value/height value) achieved was around 7, which is indicated by the line in Fig. 4. Due to the fact that the polymer ink was deposited in liquid phase, the aspect ratio is limited by the contact angle between the contact surface and the ink solution. The smallest configuration achieved had the width of 100 μm and the height of 6 μm. Various tests were performed by repeating steps 1, 2, and 5 for different widths and/or heights to fabricate the testing matrices and by filling them with colored (food color) water and ethanol, as shown in the inserted photograph in Fig. 4.

A complete prototype of a microfluidics-based flexible sensor was fabricated to demonstrate the capabilities of the proposed fabrication process, as shown in Fig. 1. To conduct the measurements, SMA connectors were mounted to the metallization using conductive epoxy, which was cured in an oven at 120 °C for 5 min, and the prototype is shown in Fig. 5(a) with its cross-section view shown in Fig. 5(b).



(a)



(b)

Fig. 5. Photographs of the fabricated proof-of-concept prototype. (a) Top view with fluid filling the channel. (b) Cross-section view.

TABLE I
PERMITTIVITY OF DIFFERENT FLUIDS AT AROUND 3 GHZ AND 300 K [22], [23], [28]

Name	Permittivity	
	Real part	Imaginary Part
Hexanol	3	1
Glycerol	4	0.4
Ethanol	6	7
Water	73	8

III. THEORY

In the natural environment, commonly utilized liquids have a wide permittivity distribution at microwave frequencies [21]–[23], as shown in Table I, while featuring different permittivity values at different temperatures or frequencies [24]–[26]. Moreover, for varying mixing ratios, mixtures of two or more fluids can feature a wide range of continuous permittivity change [25], [27]. Similarly, if any solute is added to the solvent, the permittivity of the solution varies depending on its concentration of the solute [26]. Thus, if a device is capable of detecting small changes in permittivity values of a liquid solution, it may deduce a significant amount of information about it.

To demonstrate the correlation between the permittivity value change in the microfluidic channel and the RF performance of the structure, a dual-spiral-shaped slot resonator embedded in the two ground planes of a coplanar waveguide (CPW), as shown in Fig. 6, was designed and fabricated. The chosen dual-spiral-shaped slot resonator topology features a relatively high *Q*-factor while being

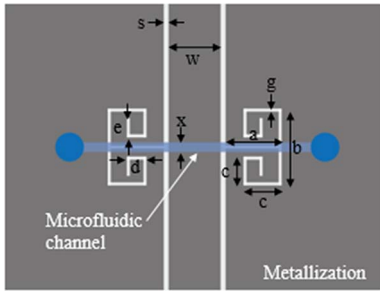


Fig. 6. Drawing of the prototype structure.

TABLE II
DIMENSIONS OF THE STRUCTURE IN FIG. 6

Parameter	Dimension (mm)	Parameter	Dimension (mm)
a	4	b	6
c	2.4	d	1.6
e	1.2	g	0.1
w	6.4	s	0.3
x	0.55		

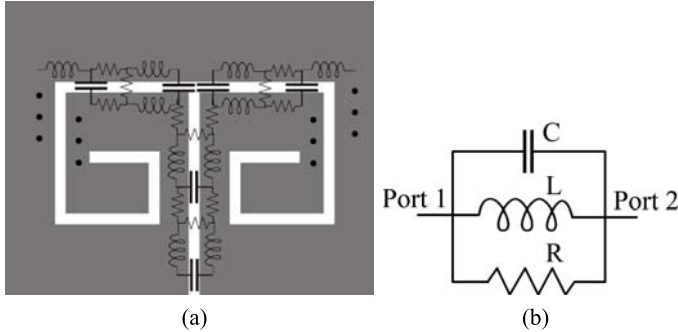


Fig. 7. Equivalent lumped circuit of the spiral-shaped slot resonator. (a) Circuit analysis of the spiral-shaped slot resonator (some duplications are clipped and represented by a dot). (b) Simplified equivalent lumped circuit.

a simple structure. The microfluidic channel is placed right on top of the longest slot to achieve a better sensitivity due to the locally stronger E -field. The geometrical parameters in Table II were optimized with an electromagnetic (EM) full-wave simulation tool (Ansoft HFSS) using the following constitutive parameters for the inkjet-printed materials of this structure: $\epsilon_r(SU8) = 3.0$, $\tan\delta(SU8) = 0.04$, $\epsilon_r(PET) = 2.9$, $\tan\delta(PET) = 0.005$ [29], $\epsilon_r(PDMS) = 2.68$, and $\tan\delta(PDMS) = 0.001$ according to the manufacturer's manual or literature. As the slot resonators are placed beside the ground conductors of a CPW transmission line, the transmitted energy over this line would be trapped in the resonator at frequencies near the resonating frequency, leading to an easy-to-detect bandstop characteristic.

The spiral-shaped slot resonator structure can be modeled using lumped elements, as shown in Fig. 7(a). Slot structures are very appropriate for microfluidics-based sensing as the permittivity value changes in the slot will drastically change its capacitance resulting in a shift of its resonant frequency, thus making it an RF parameter that could be utilized for the wireless sensing of permittivity changes. Based on the transmission-line theory and the spectral-domain approach [30], the circuit can be simplified to the parallel RLC

TABLE III
EXTRACTED PARAMETERS FOR EQUIVALENT-CIRCUIT MODEL IN FIG. 7

State of microfluidic channel	Empty Channel	Water-filled channel
Resistance R (Ω)	767.34	275.22
Capacitance C (pF)	0.80	1.68
Inductance L (nH)	2.10	3.13

circuit in Fig. 7(b) [31] and the parameters can be extracted using the following equations:

$$R = 2Z_0 \left(\frac{1}{S_{21}|_{f=f_0}} - 1 \right) \quad (1)$$

$$C = \frac{\sqrt{a^2(R + 2Z_0)^2 - 4Z_0^2}}{4\pi Z_0 R \Delta f \sqrt{1 - a^2}} \quad (2)$$

$$L = \frac{1}{4(\pi f_0)^2 C} \quad (3)$$

where f_0 is the resonant frequency, Z_0 is the 50- Ω characteristic impedance of the CPW, $S_{21}|_{f=f_0}$ is the numerical value of the insertion loss at the resonant frequency, a is the numerical value of the insertion loss at -6 -dB cutoff frequencies, and Δf is the bandwidth between two -6 -dB cutoff frequencies. Based on the measurements, the values of the equivalent lumped elements for both empty channel and water-filled channel configurations were extracted through the use of the equations above and are shown in Table III.

With the reversible sealing approach described in the fabrication section, microfluidic components with different channel sizes can be installed onto the same microwave structure to realize different sensitivities. The strength of the resonance decreases for larger frequency shifts, and there is a limit of the frequency shift above which the resonance becomes too weak to be measured [14]–[16]. So, on one hand, if a sensor has a superior sensitivity, then the shifted resonant frequency of a high-permittivity fluid may already be in the zone that has greater than -10 -dB peak attenuation. On the other hand, if a sensor can sense a large range of permittivity values, then the frequency shift per unit permittivity change would not be very large. A wide permittivity sensing range with a great sensitivity is highly desirable for practical liquid sensing designs, but it is difficult to attain. As a compromise, this “peel-and-replace” sensor is able to obtain a very wide sensing range by using a microfluidic part consisting of a small-size channel, and can have a better sensitivity while dealing with low-permittivity fluids by replacing it with a larger size channel. To investigate the influence of different channel sizes, various channel width and height values have been simulated, as shown in Fig. 8. Without loss of generality, the cross-section dimensions of $550 \mu\text{m}$ (width) \times $68 \mu\text{m}$ (height) were chosen for the prototype performance verification, as it has a relatively high sensitivity while maintaining effective resonance strength for the water-filled channel.

IV. MEASURED RESULTS

The two most important characteristics of wearable, biomonitoring, and Internet-of-Things related sensors are the

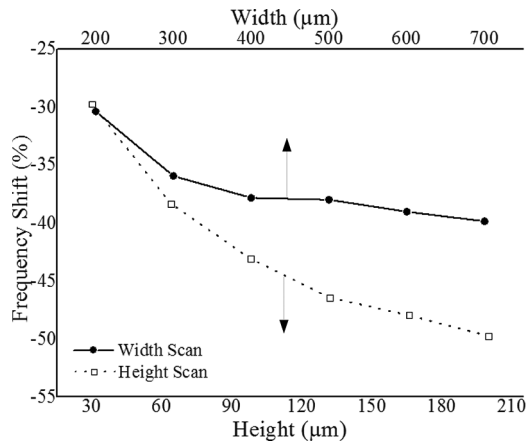


Fig. 8. Frequency shift of the resonant frequency from empty channel (permittivity = 1) to water-filled (permittivity = 73) channel for different channel dimensions. For the width scan, the height is fixed to be 68 μm . For the height scan, the width is fixed to be 550 μm .

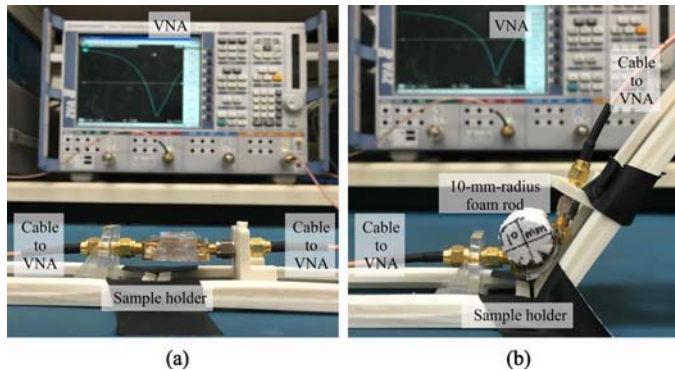


Fig. 9. Photographs of the experiment setup in: (a) flat and (b) 10-mm-radius bent configurations.

sensitivity or change in resonant frequency of the filter versus the permittivity of the fluid present in the channel, and the flexibility or repeatability and stability during bending. Therefore, the performance of the fabricated prototype was tested according to these two characteristics.

To characterize the performance of the proposed sensor, a droplet of numerous different fluids under test was dripped from the tip of a syringe to one of the two openings of the microfluidic channel. Due to the small size of the channel, capillary action happens: when a dry channel opening is brought into contact with a liquid, it will imbibe the liquid at a rate that decreases with time. As the channel has the same size all the way between the two openings and the device prototype is placed horizontally so that gravity’s effect is negligible, the liquid would flow into the channel and fill the channel automatically. In this way, no microfluidic connector, pump, or tube is needed, but only a droplet of the fluid, thus simplifying the system while saving the bulk of the fluids under test. Due to the hydrophobic property of SU-8 and PDMS, the electrical and microfluidic parts were treated separately for 5 min in a UVO cleaner before filling water into the channel. Between consecutive tests with the same or different liquids, the two parts were demounted, cleaned by dry cool air flow and mounted together again. A Rhode and Schwartz ZVA-8 vector network analyzer (VNA) was used

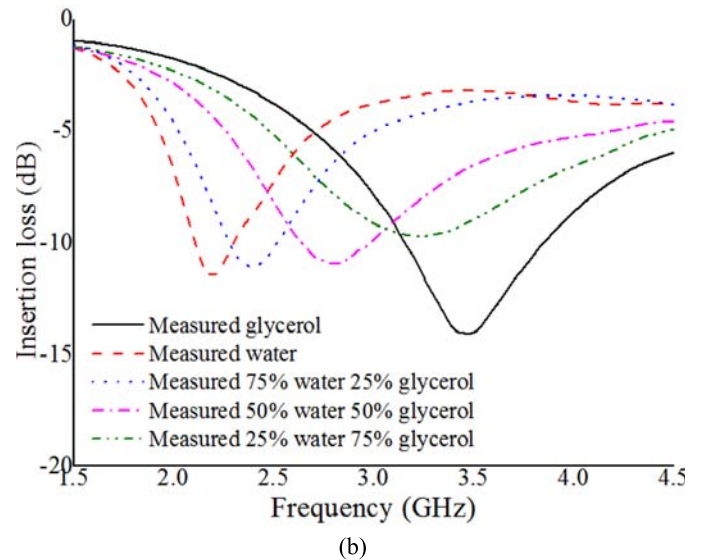
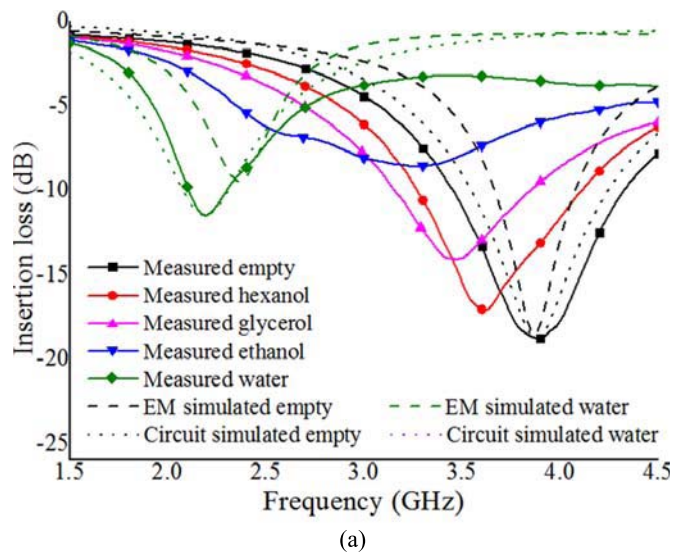


Fig. 10. (a) Measured insertion-loss values of the proposed RF sensor for four different fluids in the channel, as well as for an empty channel, along with EM (HFSS) simulated and circuit (ADS) simulated results for an empty and a water-filled channel. (b) Measured insertion-loss values for a glycerol–water mixture with different mixing ratios in the channel, which verifies the capability to clearly distinguish mixtures with different mix ratios.

to measure the S-parameters of the device prototype under various fluids and bending conditions.

A. Sensitivity

In order to demonstrate the sensitivity of the proposed device prototype, several different fluids or fluid mixtures were used, namely, water, ethanol, glycerol, hexanol, and water-glycerol mixtures with three different mixing ratios, which feature a wide distribution of relative permittivity values from 1 to 73, as shown in Table I. The sensor prototype was held above the ground to minimize the ground interference effects and to ensure the same measurement configuration for different liquids under test, as shown in Fig. 9(a).

The simulated and measured values of the insertion loss of the proposed resonator for different fluids in the channel can be found in Fig. 10. A very significant frequency shift when replacing hexanol ($\epsilon_r = 3$) with glycerol ($\epsilon_r = 4$)

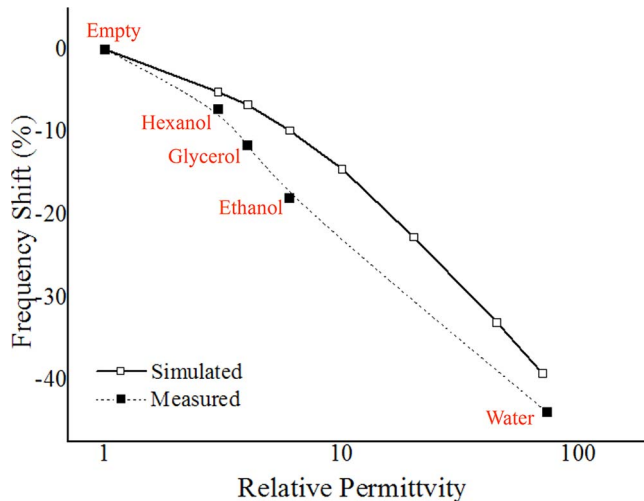


Fig. 11. Measured and simulated values of the resonant frequency shift for different relative permittivity fluids into the channel, demonstrating a logarithmic linearity of the sensor prototype.

can be observed, though the relative permittivity difference is barely 1 and the cross section of the proposed sensing channel is as small as $5.4 \times 10^{-6} \times \lambda_0^2$. The variance of the stopband attenuation and of the bandwidth for the different fluids filled channel is due to the dielectric loss of various fluids and the mismatches as the frequency shifted largely. In Fig. 11, a good logarithmic linearity can be observed in both simulations and measurements at around $-24\%/\log(\epsilon_r)$. Due to the tiny size of the channel, only $0.6358\text{-}\mu\text{L}$ fluid is needed to fill, which results in a sensitivity around $37\%/\log(\epsilon_r)/\mu\text{L}$. Any $0.4 \log(\epsilon_r)$ change will lead to a frequency shift larger than one 3-dB bandwidth (10% for low-loss fluids), while the sensor resolution heavily relies on the system's resolution. The higher resolution of analog-to-digital converter, the smaller frequency sweep step, and the lower noise of source, the better the sensor resolution. The resonant frequency of the bandstop filter is shifted by 43.8% in Fig. 10 from 3.9 to 2.19 GHz when an empty channel is replaced with a water-filled channel. To the best of authors' knowledge, this sensor prototype features the highest sensitivity compared with other recently published microwave/RF microfluidic sensors, including inkjet-printed sensors (e.g., 28% from empty to water reported in [14]), as well as sensors fabricated by traditional soft lithography methods (e.g., 21% from empty to water reported in [9]).

B. Flexibility

In addition to good sensitivity, endurance as well as a consistently good performance for different bending conditions is significant. To test the performance under a bending status, the sensor prototype was folded around four low-dielectric ($\epsilon_r < 2$) cylinders with four different radii: 7, 10, 27, and 35 mm. An example of an experimental setup for a bent configuration with a 10-mm radius is shown in Fig. 9(b). The comparison between the insertion-loss values for the configurations of an empty channel ($\epsilon_r = 1$) and a water-filled channel ($\epsilon_r = 73$) for the four different cylinders and for the

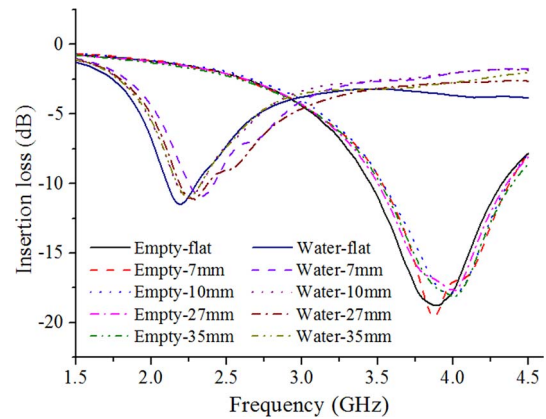


Fig. 12. Measured insertion-loss values of the proposed flexible wireless liquid sensor prototype for empty and water-filled channel configurations and for different radii of curvature.

flat configuration is shown in Fig. 12. Less than 130-MHz resonant frequency shifts and a smaller than 1.1-dB insertion-loss variation are observed verifying a reliable performance for both bent and flat mounting conditions. After bending 30 times, the insertion loss of the sensor prototype in the flat configuration was measured again and was very close to the initial measurements, demonstrating a good reusability and reliability between pre-/post-bending performance.

V. CONCLUSION

This paper has demonstrated a novel low-cost low-temperature zero-waste approach to manufacture flexible microfluidics-based RF devices on virtually every substrate by combining inkjet printing and soft lithography. A reusable and flexible microfluidics sensor prototype fabricated with this process was presented and featured a very good performance. The unique "peel-and-replace" capability of the proposed structure allows for an easier cleaning process facilitating reusability, as well as a reconfigurable sensitivity/measured permittivity value range. For a microfluidic sensor requiring less than $1 \mu\text{L}$ of the liquid under test and a cross-section of the channel as small as $5.4 \times 10^{-6} \times \lambda_0^2$, seven different fluids were used to evaluate the prototype's performance, effectively featuring a sensitivity of $24\%/\log(\epsilon_r)$, a higher value compared to other state-of-the-art microfluidics-based RF sensors. At the same time, the proposed sensor maintains a very good functionality even for a bending radius of 7 mm, making the proposed approach a very good candidate for the fabrication of wearable, biomonitoring, mountable, food quality monitoring, "smart skins," and Internet-of-Things wireless modules.

REFERENCES

- [1] A. Pantelopoulou and N. G. Bourbakis, "A survey on wearable sensor-based systems for health monitoring and prognosis," *IEEE Trans. Syst., Man, Cybern. C, Appl. Rev.*, vol. 40, no. 1, pp. 1–12, Jan. 2010.
- [2] Y. Hao and R. Foster, "Wireless body sensor networks for health-monitoring applications," *Physiol. Meas.*, vol. 29, no. 11, p. R27, 2008.
- [3] D. Diamond, S. Coyle, S. Scarmagnani, and J. Hayes, "Wireless sensor networks and chemo-/biosensing," *Chem. Rev.*, vol. 108, no. 2, pp. 652–679, 2008.

- [4] D. R. Reyes, D. Iossifidis, P.-A. Auroux, and A. Manz, “Micro total analysis systems. 1. Introduction, theory, and technology,” *Anal. Chem.*, vol. 74, no. 12, pp. 2623–2636, 2002.
- [5] F. Benito-Lopez, S. Coyle, R. Byrne, and D. Diamond, “Sensing sweat in real-time using wearable microfluidics,” in *Proc. 7th Int. Wearable Implantable Body Sensor Netw. Workshop*, Singapore, 2010, pp. 31–33.
- [6] G. M. Whitesides, “The origins and the future of microfluidics,” *Nature*, vol. 442, no. 7101, pp. 368–373, 2006.
- [7] G. M. Whitesides and A. D. Stroock, “Flexible methods for microfluidics,” *Phys. Today*, vol. 54, no. 6, pp. 42–48, 2001.
- [8] D. C. Duffy, J. C. McDonald, O. J. Schueller, and G. M. Whitesides, “Rapid prototyping of microfluidic systems in poly (dimethylsiloxane),” *Anal. Chem.*, vol. 70, no. 23, pp. 4974–4984, 1998.
- [9] A. Ebrahimi, W. Withayachumnankul, S. Al-Sarawi, and D. Abbott, “High-sensitivity metamaterial-inspired sensor for microfluidic dielectric characterization,” *IEEE Sensors J.*, vol. 14, no. 5, pp. 1345–1351, May 2014.
- [10] J. N. Lee, C. Park, and G. M. Whitesides, “Solvent compatibility of poly (dimethylsiloxane)-based microfluidic devices,” *Anal. Chem.*, vol. 75, no. 23, pp. 6544–6554, 2003.
- [11] K. Abe, K. Suzuki, and D. Citterio, “Inkjet-printed microfluidic multianalyte chemical sensing paper,” *Anal. Chem.*, vol. 80, no. 18, pp. 6928–6934, 2008.
- [12] C. Mariotti, W. Su, B. S. Cook, L. Roselli, and M. M. Tentzeris, “Development of low cost, wireless, inkjet printed microfluidic RF systems and devices for sensing or tunable electronics,” *IEEE Sensors J.*, vol. 15, no. 6, pp. 3156–3163, Jun. 2015.
- [13] B. S. Cook, J. R. Cooper, and M. M. Tentzeris, “An inkjet-printed microfluidic RFID-enabled platform for wireless lab-on-chip applications,” *IEEE Trans. Microw. Theory Techn.*, vol. 61, no. 12, pp. 4714–4723, Dec. 2013.
- [14] W. Su, C. Mariotti, B. Cook, S. Lim, L. Roselli, and M. Tentzeris, “A metamaterial-inspired temperature stable inkjet-printed microfluidic-tunable bandstop filter,” in *IEEE 44th Eur. Microw. Conf.*, 2014, pp. 9–12.
- [15] W. Su, B. Cook, M. Tentzeris, C. Mariotti, and L. Roselli, “A novel inkjet-printed microfluidic tunable coplanar patch antenna,” in *IEEE Antennas Propagat. Soc. Int. Symp.*, 2014, pp. 858–859.
- [16] W. Su, B. Cook, and M. M. Tentzeris, “A low-cost inkjet-printed microfluidics-based tunable loop antenna fed by microfluidics-based tunable balun,” in *9th Eur. Antennas Propag. Conf.*, Lisbon, Portugal, Apr. 2015, 4 pp.
- [17] B. Cook, J. Cooper, and M. Tentzeris, “Multi-layer RF capacitors on flexible substrates utilizing inkjet printed dielectric polymers,” *IEEE Microw. Wireless Compon. Lett.*, vol. 23, no. 7, pp. 353–355, Jul. 2013.
- [18] B. S. Cook, B. Tehrani, J. R. Cooper, and M. M. Tentzeris, “Multilayer inkjet printing of millimeter-wave proximity-fed patch arrays on flexible substrates,” *IEEE Antennas Wireless Propag. Lett.*, vol. 12, pp. 1351–1354, 2013.
- [19] R. Yang and W. Wang, “A numerical and experimental study on gap compensation and wavelength selection in UV-lithography of ultra-high aspect ratio SU-8 microstructures,” *Sens. Actuators B, Chem.*, vol. 110, no. 2, pp. 279–288, 2005.
- [20] M. Nordström, R. Marie, M. Calleja, and A. Boisen, “Rendering SU-8 hydrophilic to facilitate use in micro channel fabrication,” *J. Micromechan. Microeng.*, vol. 14, no. 12, pp. 1614–1617, 2004.
- [21] A. Tidar *et al.*, “Microwave dielectric relaxation study of 1-hexanol with 1-propanol mixture by using time domain reflectometry at 300 K,” in *Appl. Electromagn. Conf.*, Dec. 2009, pp. 1–4.
- [22] R. Nigmatullin, M. A.-G. Jafar, N. Shinyashiki, S. Sudo, and S. Yagihara, “Recognition of a new permittivity function for glycerol by the use of the eigen-coordinates method,” *J. Non-Crystal. Solids*, vol. 305, pp. 96–111, 2002.
- [23] K. Shibata, “Measurement of complex permittivity for liquid materials using the open-ended cut-off waveguide reflection method,” in *Proc. Joint China–Japan Microw. Conf.*, Apr. 2011, pp. 1–4.
- [24] A. E. Lipton, M. K. Griffin, and A. G. Ling, “Microwave transfer model differences in remote sensing of cloud liquid water at low temperatures,” *IEEE Trans. Geosci. Remote Sens.*, vol. 37, no. 1, pp. 620–623, Jan. 1999.
- [25] G. Akerlof, “Dielectric constants of some organic solvent-water mixtures at various temperatures,” *J. Amer. Chem. Soc.*, vol. 54, no. 11, pp. 4125–4139, 1932.
- [26] R. Somaraju and J. Trunpf, “Frequency, temperature and salinity variation of the permittivity of seawater,” *IEEE Trans. Antennas Propag.*, vol. 54, no. 11, pp. 3441–3448, Nov. 2006.
- [27] R. Behrends, K. Fuchs, U. Kaatz, Y. Hayashi, and Y. Feldman, “Dielectric properties of glycerol/water mixtures at temperatures between 10 and 50 C,” *J. Chem. Phys.*, vol. 124, no. 14, p. 144512, 2006.
- [28] P. Petong, R. Pottel, and U. Kaatz, “Dielectric relaxation of h-bonded liquids. Mixtures of ethanol and n-hexanol at different compositions and temperatures,” *J. Phys. Chem. A*, vol. 103, no. 31, pp. 6114–6121, 1999.
- [29] J. Bellomo and T. Lebey, “On some dielectric properties of pen,” *J. Phys. D, Appl. Phys.*, vol. 29, no. 7, p. 2052, 1996.
- [30] C.-C. Chang, C. Caloz, and T. Itoh, “Analysis of a compact slot resonator in the ground plane for microstrip structures,” in *Proc. Asia–Pacific Microw. Conf.*, 2001, vol. 3, pp. 1100–1103.
- [31] H. Liu, T. Yoshimasu, and L. Sun, “CPW bandstop filter using periodically loaded slot resonators,” *Electron. Lett.*, vol. 42, no. 6, pp. 352–353, 2006.



Wenjing Su (S’14) was born in Hunan, China, in 1991. She received the B.S. degree in electrical engineering from the Beijing Institute of Technology, Beijing, China, in 2013, and is currently working toward the Ph.D. degree in electrical and computer engineering at the Georgia Institute of Technology, Atlanta, GA, USA.

In Fall 2013, she joined the ATHENA Research Group, Georgia Institute of Technology, as a Graduate Research Assistant. Her research is focused on additively manufactured microfluidics sensors for Internet of Things (IoT) and wireless/distributed healthcare applications, as well as tunable antennas and passive RF components for wideband/reconfigurable communication system. Her works covers the entire development cycle including improvement of the fabrication process, microwave/RF sensor component design, and high-frequency characterization and measurements.

Ms. Su was the recipient of the Honors Class Program Scholarship and the People’s Scholarship of the Beijing Institute of Technology (2009–2013). She was also the recipient of the IEEE Microwave Theory and Techniques Society (IEEE MTT-S) International Microwave Symposium (IMS) Ph.D. Student Sponsorship Initiative in 2014.



Benjamin S. Cook (GSM’12) received the B.Sc. degree in electrical engineering from the Rose-Hulman Institute of Technology, Terre Haute, IN, USA, in 2010, the M.A.Sc. degree in electrical engineering from the King Abdullah University of Science and Technology, Thuwal, Saudi Arabia, in 2011, and the Ph.D. degree in electrical engineering from the Georgia Institute of Technology, Atlanta, GA, USA, in 2014.

He is currently a Research Scientist with Kilby Labs, Texas Instrument Incorporated, Dallas, TX, USA. He has authored or coauthored over 25 peer-reviewed publications. His research is focused on inkjet process design for vertically integrated millimeter-wave devices, system-on-paper applications, green electronics, microelectromechanical systems (MEMS) device fabrication, RF energy harvesting and passive wireless sensors.

Dr. Cook was the recipient of the Outstanding Senior Electrical and Computer Engineering Student of the Year Award of the Rose-Hulman Institute of Technology, the King Abdullah University of Science and Technology (KAUST) Fellowship Award in 2010, and the KAUST Provost Award in 2011. During the course of his Ph.D. work, he was the recipient of the IEEE Antennas and Propagation Society Doctoral Research Award and the Intel Doctoral Fellowship for his work in vertically integrated inkjet fabrication for millimeter-wave applications.



Manos M. Tentzeris (S'89–M'92–SM'03–F'10) received the Diploma degree in electrical and computer engineering (*magna cum laude*) from the National Technical University of Athens, Athens, Greece, and the M.S. and Ph.D. degrees in electrical engineering and computer science from the University of Michigan, Ann Arbor, MI, USA.

He is currently a Professor with the School of Electrical and Computer Engineering, Georgia Institute of Technology, Atlanta, GA, USA. He has helped develop academic programs in highly integrated/multilayer packaging for RF and wireless applications using ceramic and organic flexible materials, paper-based RF identifications (RFIDs) and sensors, biosensors, wearable electronics, inkjet-printed electronics, “green” electronics and power scavenging, nanotechnology applications in RF, microwave microelectromechanical systems (MEMS), system-on-package (SOP)-integrated (ultra-wideband (UWB), multiband, millimeter-wave (mmW), conformal) antennas and heads the ATHENA Research Group (20 researchers), Georgia Institute of Technology. From 2006 to 2010, he served as the Georgia Electronic Design Center Associate Director for RFID/Sensors Research and, from 2003 to 2006, as the Georgia Institute of Technology NSF-Packaging Research Center Associate Director for RF Research and the RF Alliance Leader. In the summer of 2002, he was a Visiting Professor with the Technical University of Munich, Munich, Germany. In the summer of 2009, he was a Visiting Professor with GTRI-Ireland, Athlone, Ireland. In the summer of 2010, he was a Visiting Professor with LAAS-CNRS, Toulouse, France. He has given more than 100 invited talks to various universities and companies all over the world. He has authored or coauthored more than 580 papers in refereed journals and conference proceedings, 5 books, and 21 book chapters.

Dr. Tentzeris is a Member of the URSI-Commission D and the MTT-15 Committee. He is an Associate Member of the European Microwave Association (EuMA). He is a Fellow of the Electromagnetic Academy. He is a Member of the Technical Chamber of Greece. He served as an IEEE Microwave Theory and Techniques Society (IEEE MTT-S) Distinguished Microwave Lecturer (2010–2012). He is currently a Distinguished

Lecturer of the IEEE Council on RFIDs (CRFID). He was the Technical Program Committee (TPC) Chair for the IEEE MTT-S International Microwave Symposium (IMS) 2008 and the Chair of the 2005 IEEE CEM-TD Workshop. He is the Vice-Chair of the RF Technical Committee (TC16) of the IEEE CPMT Society. He was the founder and has been the Chair of the RFID Technical Committee (TC24), IEEE MTT-S and the Secretary/Treasurer of the IEEE C-RFID. He has served as an Associate Editor for the IEEE TRANSACTIONS ON MICROWAVE THEORY AND TECHNIQUES, IEEE TRANSACTIONS ON ADVANCED PACKAGING, and the *International Journal on Antennas and Propagation*. He was the recipient/corecipient of the 2015 IET Microwaves, Antennas and Propagation Premium Award, the 2014 Georgia Institute of Technology Electrical and Computer Engineering Distinguished Faculty Achievement Award, the 2014 IEEE RFID-TA Best Student Paper Award, the 2013 IET Microwaves, Antennas and Propagation Premium Award, the 2012 FiDiPro Award in Finland, the iCMG Architecture Award of Excellence, the 2010 IEEE Antennas and Propagation Society Piergiorgio L. E. Uslenghi Letters Prize Paper Award, the 2011 International Workshop on Structural Health Monitoring Best Student Paper Award, the 2010 Georgia Institute of Technology Senior Faculty Outstanding Undergraduate Research Mentor Award, the 2009 IEEE TRANSACTIONS ON COMPONENTS AND PACKAGING TECHNOLOGIES Best Paper Award, the 2009 E. T. S. Walton Award from the Irish Science Foundation, the 2007 IEEE AP-S Symposium Best Student Paper Award, the 2007 IEEE MTT-S IMS Third Best Student Paper Award, the 2007 ISAP 2007 Poster Presentation Award, the 2006 IEEE MTT-S Outstanding Young Engineer Award, the 2006 Asian-Pacific Microwave Conference Award, the 2004 IEEE TRANSACTIONS ON ADVANCED PACKAGING Commendable Paper Award, the 2003 NASA Godfrey “Art” Anzic Collaborative Distinguished Publication Award, the 2003 IBC International Educator of the Year Award, the 2003 IEEE CPMT Outstanding Young Engineer Award, the 2002 International Conference on Microwave and Millimeter-Wave Technology Best Paper Award, Beijing, China, the 2002 Georgia Institute of Technology Electrical and Computer Engineering Outstanding Junior Faculty Award, the 2001 ACES Conference Best Paper Award, and the 2000 National Science Foundation (NSF) CAREER Award and the 1997 Best Paper Award of the International Hybrid Microelectronics and Packaging Society.